

# Flow and transport in the unsaturated Sherwood Sandstone: characterization using cross-borehole geophysical methods

PETER WINSHIP, ANDREW BINLEY & DIEGO GOMEZ

*Department of Environmental Science, Lancaster University, Lancaster LA1 4YQ, UK  
(e-mail: A.Binley@lancaster.ac.uk)*

**Abstract:** Cross-borehole radar and resistivity measurements have been used to characterize changes in moisture content and solute concentration due to controlled injection of 1200 l of a saline tracer in the unsaturated zone of the Sherwood Sandstone at a field site in Yorkshire, UK. Borehole radar transmission profiles show the vertical migration of the wetting front during the tracer test. Three-dimensional cross-borehole electrical resistivity tomography was deployed to monitor changes over time in resistivity, caused by the increase in moisture content and pore-water salinity due to the tracer. The results show clearly the development of the tracer plume as it migrates towards the water table at a depth of 10 m. The tomographic results reveal the impact of a hydraulically impeding layer between a depth of 8 and 9 m. Geophysical and geological logs acquired at the site support this conceptualization. By combining the resistivity tomograms with cross-borehole radar tomograms, changes in pore-water concentration over time have been estimated. Changes in moisture content inferred from the geophysical results were compared with those produced by a three-dimensional unsaturated flow model. Using a sandstone effective hydraulic conductivity of  $0.4 \text{ m day}^{-1}$  in the model produced moisture profiles over time that were comparable with those inferred from the geophysical data during the early stages of the tracer test. Differences between modelled and field results were attributed to the impact of hydraulically impeding layers of finer sediments within the profile.

The ability to predict reliably the travel time of diffuse and point-source contaminants through the unsaturated zone of the Sherwood Sandstone is essential for the management of this nationally important water resource. Field characterization of flow and transport in the unsaturated zone is necessary in order to understand fully the natural processes that affect the fate of contaminants before they reach the water table. Traditionally, borehole-based sampling methods have been used to monitor transport processes in the subsurface. These methods are limited in that the measurement support volume is typically constrained to tens of cubic centimetres. In the unsaturated zone, the application of such methods is complicated by the need to extract pore-water samples at appropriate negative pressures (suctions) in order to obtain samples that truly represent the entire pore-size distribution.

Geophysical techniques have been widely used in hydrogeological studies for decades. For example, Rubin & Hubbard (2005) present the theoretical links between hydrological properties and geophysical parameters, and, through a wide range of case studies, highlight the potential hydrological value gained from geophysical surveys. Several methods, in particular resistivity

and radar, allow high-resolution spatial and temporal sampling of the subsurface environment. The characterization of the shallow subsurface has been demonstrated by numerous applications of these methods; however, only recently have attempts been made to quantify directly hydrogeological properties using these techniques (Rubin & Hubbard 2005).

In 1998 a joint project between the universities of Lancaster and Leeds, funded by the UK Natural Environment Research Council and the UK Environment Agency, was initiated to examine, using geophysical methods, unsaturated flow and transport processes at two purposely developed field sites in the UK Sherwood Sandstone. This work, so far, has demonstrated: how cross-borehole (borehole to borehole) radar tomography can be used to monitor changes in moisture content in the unsaturated zone due to natural and forced (tracer) inputs (Binley *et al.* 2001); the evaluation of seasonal variation of moisture content profiles using high-resolution borehole resistivity and radar profiling (Binley *et al.* 2002*b*); initial attempts to utilise the geophysical data to develop numerical predictive models of unsaturated flow (Binley *et al.* 2002*a*; Binley & Beven 2003; Binley *et al.* 2004). In addition,

petrophysical models relating geophysical data to hydrological properties have been developed (West *et al.* 2003). These articles have concentrated on monitoring and modelling moisture content variation. We report here on a recent joint hydrological–geophysical study of flow and transport in the Sherwood Sandstone at one of the field sites.

The two techniques used here are three-dimensional time-lapse electrical resistivity tomography (ERT) and time-lapse cross-borehole radar tomography and profiling. They provide geophysical measurements that can be related to the moisture content of the subsurface, and subsequently to the conductivity of that moisture content. They also yield data on a scale that is appropriate for numerical simulations of water movement in the subsurface. The two methods have been applied at a site (Lings Farm, Hatfield, near Doncaster, UK) on the outcrop of the Sherwood Sandstone (Fig. 1).

#### *Cross-borehole radar and resistivity: basic concepts*

In cross-borehole ERT, four-electrode resistance measurements are made using electrodes in two or more boreholes. Often surface electrodes are used to supplement the electrode array. Inversion of the resistance data is necessary in order to determine an image of resistivity between the boreholes. By discretizing the domain of interest into parameter cells, the objective of the inversion procedure is to compute the ‘best’ set of resistivity values that satisfies both the measured data set and any *a priori* constraints.

The inversion approach normally adopted uses regularization to stabilize the inversion and constrain the final image (e.g. LaBrecque *et al.* 1996). Cross-borehole ERT has been demon-

strated in a wide range of environments. One of the earliest examples of hydrological applications of ERT is Daily *et al.* (1992) in a study of vadose zone moisture migration due to application of a tracer. Other examples of unsaturated zone studies using ERT include Slater *et al.* (1997), Ramirez & Daily (2001) and French *et al.* (2002). At the Hatfield site, Binley *et al.* (2002a) demonstrated how three- and two-dimensional ERT can be used successfully to monitor changes in moisture content in the unsaturated sandstone.

Borehole-to-borehole radar surveys may be conducted in two transmission modes in order to determine dielectric properties at the field scale. In both cases a radar signal is transmitted from one antenna placed in the first borehole and received by a second antenna in the other borehole. Measurement of the received electromagnetic wave permits determination of the first arrival and hence velocity of the wave ( $v$ ). In one mode, using a multiple offset gather (MOG), the receiver is moved to different locations in one borehole whilst the transmitter remains fixed (Peterson 2001). The transmitter is then moved and the process repeated. Following collection of all data in this mode and determination of the travel time for each wave path-line it is possible to derive a tomogram of velocity within the plane of the borehole pair. In contrast, a zero offset profile (ZOP) may be determined by keeping both the transmitter and receiver at equal depth. By systematically lowering or raising the pair of antennae in the two boreholes it is possible to build a one-dimensional profile of average inter-borehole travel time over the entire borehole length.

Examination of the wave-form of the received signal allows the travel time, and hence the velocity of a radar wave, through the material between the boreholes to be determined. In low loss materials and at high frequency, the real part of the bulk dielectric constant ( $\kappa$ ) is derived from:

$$\sqrt{\kappa} = \frac{c}{v} \quad (1)$$

where  $c$  is the radar wave velocity in air ( $\approx 0.3 \text{ m ns}^{-1}$ ).

The increasing availability of commercial borehole radar systems and growing acceptance of radar in the hydrological community has led to a number of recent hydrogeological applications of the technique in unsaturated systems (e.g. Hubbard *et al.* 1997; Alumbaugh *et al.* 2002; Galagedera *et al.* 2003).

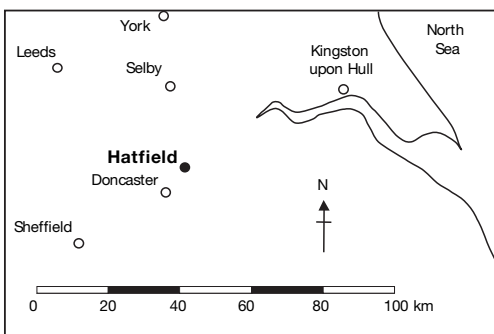


**Fig. 1.** Hatfield site location.

## Site description

At the Hatfield site six boreholes were drilled in 1998 in order to monitor tracers injected into the sandstone (Fig. 2). Four of these boreholes (H-E1, H-E2, H-E3 and H-E4) were designed for resistivity measurements. These ERT boreholes contain 16 stainless steel mesh electrodes equally spaced at depths of between 2 and 13 m. Two boreholes (H-R1 and H-R2) were installed for radar measurements. These boreholes were drilled to a depth of 12 m and completed with 75 mm PVC casing. Both the ERT and radar boreholes have a weak sand–cement grout backfilling the gap between the host formation and installation. A tracer injection borehole (H-I2) was also installed within the centre of the borehole array (Fig. 2). The injection borehole is 3.5 m deep, with a 100 mm-diameter slotted section, and gravel pack between 3 and 3.5 m in depth.

Two cored boreholes were drilled at the site (Fig. 2) and logged by Leeds University (Pokar *et al.* 2001) (Fig. 3). The main lithology present in the core is medium-grained sandstone, interspersed with interlaminated fine- and medium-grained sandstones, particularly in the zone around 6 m depth, and between 8 and 9 m. Drift at the top of the section at the site is typically 2–3 m thick, and consists mainly of fluvio-glacial sands, derived from the underlying sandstones, with frequent large pebbles/cobbles.

In order to minimize disturbance, particularly from ingress of drilling fluids, cores were not extracted from the tracer array area. However, geophysical logs were obtained for all drilled boreholes using electromagnetic induction and natural gamma logging tools. Figure 4 shows example natural gamma logs for the boreholes H-E2, H-R2, H-R2 and H-E1. These logs reveal

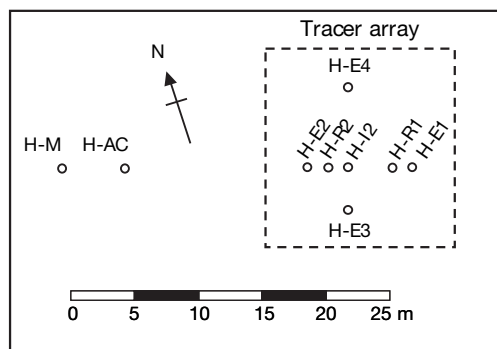


Fig. 2. Field site layout showing boreholes.

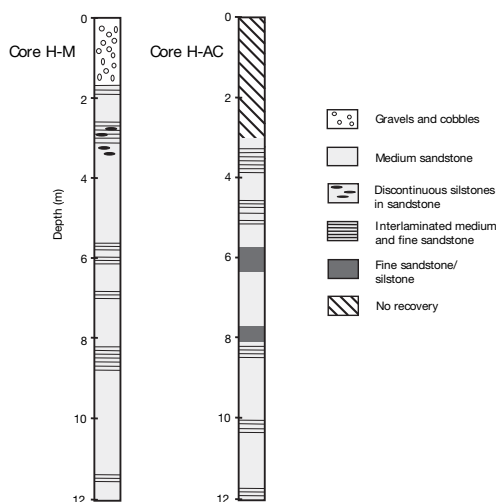


Fig. 3. Core logs (supplied by J. West, Leeds University).

subtle contrasts but support the conceptualization of repeated fine–medium sandstone layering.

## Experimental procedures

During March 2003 a saline tracer was injected into the sandstone using borehole H-I2. Changes in bulk resistivity and dielectric constant of the sandstone were then monitored using radar and resistivity using the procedures described below.

### Cross-borehole ERT

In order to compute a high-resolution image of the subsurface using cross-borehole ERT it is necessary to acquire a large number of four electrode measurements. During tracer tests the data capture time is critical, as each image should reflect a ‘snapshot’ of the subsurface. For this experiment, a six-channel Geoserve Resecs instrument was used, allowing the collection of 6372 measurements in about 2.5 h. The current and potential electrode pairs were chosen so that the dipoles they defined were horizontal, with one of the electrodes in each dipole being in one borehole and the other in any of the remaining three boreholes. The current and potential dipoles were restricted to being within 4.4 m of each other vertically, so that measured voltages were not too low. For all ERT surveys, reciprocal data (i.e. with current and potential electrodes swapped) were collected to assess

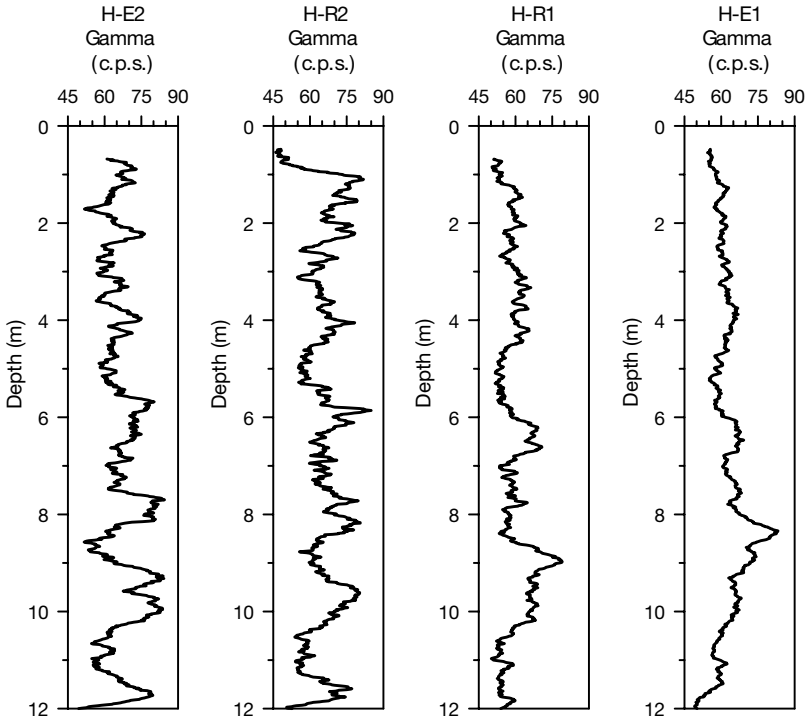


Fig. 4. Natural gamma logs in boreholes H-E2, H-R2, H-R1 and H-E1.

error levels (repeatability checks are often inadequate for this purpose: Daily *et al.* 2004). Thus, a maximum of 3186 measurements were used for data inversion. Inversion of the data in order to produce a three-dimensional resistivity tomogram was based on a regularized least-squares algorithm similar to that outlined in Morelli & LaBrecque (1996).

Resistivity values so obtained are assumed here to be related to hydrogeological parameters by Archie's Law (Archie 1942):

$$\rho = a\phi^{-m} \left( \frac{\theta}{\phi} \right)^{-n} \rho_w \quad (2)$$

where  $\rho$  is the resistivity of the bulk material,  $\phi$  is the porosity,  $\rho_w$  is the resistivity of the pore fluid,  $\theta$  the volumetric moisture content, and  $a$ ,  $m$  and  $n$  are formation constants. For resistivity measurements repeated at different times, then:

$$\frac{\rho_t}{\rho_0} = \frac{\theta_t^{-n} \rho_{w,t}}{\theta_0^{-n} \rho_{w,0}} \quad (3)$$

where the subscripts  $t$  and  $0$  refer to measurements at time  $t$  and time  $0$ , respectively.

We recognize the limitation of using Archie's

law in shaly sandstone (see, for example, Worthington 1977), but in the absence of appropriate petrophysical relationships the Archie model is adopted as a suitable first approximation.

#### Cross-borehole radar

Using boreholes H-R1 and H-R2, two radar data collection modes were adopted: zero offset profiling (ZOP) and multiple offset gathers (MOG). For both surveys a Sensors and Software Pulse EKKO PE100 system was used with 100 MHz antennae. For the ZOP surveys the antennae were lowered at 0.25 m increments. For the MOG surveys a 'complete' data set was not obtained due to time constraints imposed by the expected tracer movement. The MOG surveys carried out used transmitter locations at 1 m increments between depths of 1 and 10 m in H-R1, with receiver positions at 0.25 m increments between 1 and 10 m depth in H-R2 (also ensuring that the absolute vertical angle between transmitter and receiver did not exceed  $45^\circ$ ). MOG data were inverted using the MIGRATOM code (Jackson & Tweeton 1994) to produce an image of radar velocity between

H-R1 and H-R2 and hence, using equation 1, an image of the bulk dielectric constant.

In order to describe the relationship between bulk dielectric constant and volumetric moisture content the complex refractive index method (CRIM) was used. The CRIM model can be stated as:

$$\sqrt{\kappa} = (1 - \phi)\sqrt{\kappa_s} + \theta\sqrt{\kappa_w} + (\phi - \theta)\sqrt{\kappa_a} \quad (4)$$

where  $\kappa_s$  is the dielectric constant of the sediment grains,  $\kappa_w$  is the dielectric constant of water (assumed to be 81),  $\kappa_a$  is the dielectric constant of air (assumed to be 1) and  $\phi$  is porosity. West *et al.* (2003) carried out measurements of dielectric properties at different levels of water saturation in core samples extracted from the site. Based on these measurements we assume here that  $\kappa_s = 5$  and  $\phi = 0.32$ . Note that the dielectric constant is independent of the electrical conductivity of the pore fluid.

Where measurements are taken at different times, equations 1 and 4 can be used to give the change in moisture content ( $\Delta\theta$ ) as a function of the difference in observed radar wave velocity ( $\Delta v$ ):

$$\Delta\theta = \Delta v \left( \frac{c}{\sqrt{\kappa_a} - \sqrt{\kappa_w}} \right). \quad (5)$$

*The tracer experiment*

The tracer consisted of 1200 l of water, dosed with NaCl to give an electrical conductivity of 2200  $\mu\text{S cm}^{-1}$  (groundwater electrical conductivity at the site was measured as 650  $\mu\text{S cm}^{-1}$ ). The tracer was injected over a period of 3 days, from 14 to 17 March 2003, at a steady rate of approximately 17 l  $\text{h}^{-1}$ . A float valve in the injection borehole was used to control the head in the injection borehole, and hence the flow rate. Duplicate sets of background measurements of ERT were made on 6 and 13 March, and of radar measurements on 6 and 14 March. Tracer flow was monitored by means of a pressure transducer in a storage tank, which gave a way of calculating the cumulative injection volume over time. During the tracer test no rainfall was observed at the site. The water table was observed at approximately 10 m depth.

**Results and analysis**

Figure 5 shows the background (pre-tracer) ZOP results, converted to dielectric constant. Assuming that the dielectric constant is principally controlled by the moisture content, the

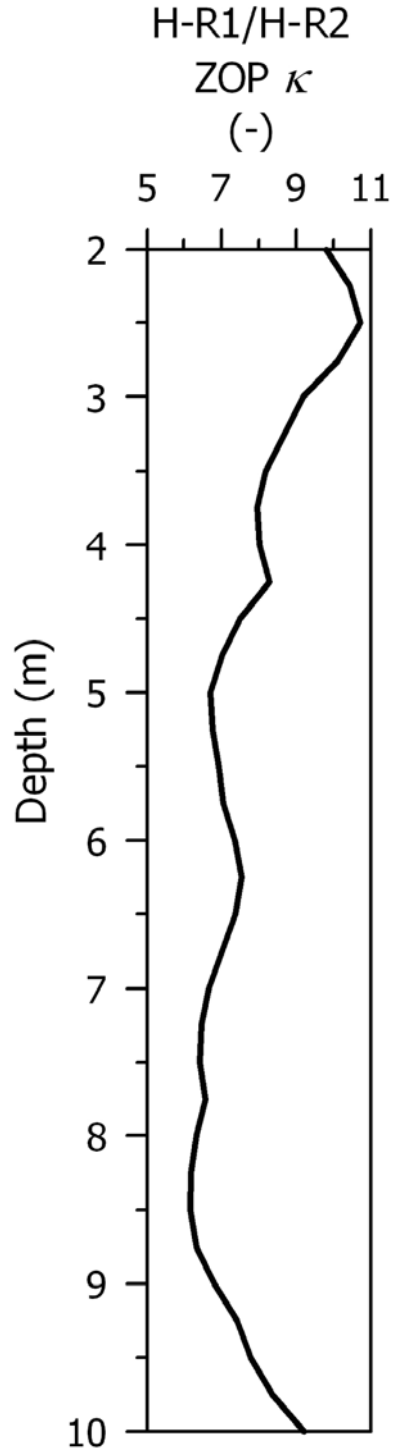
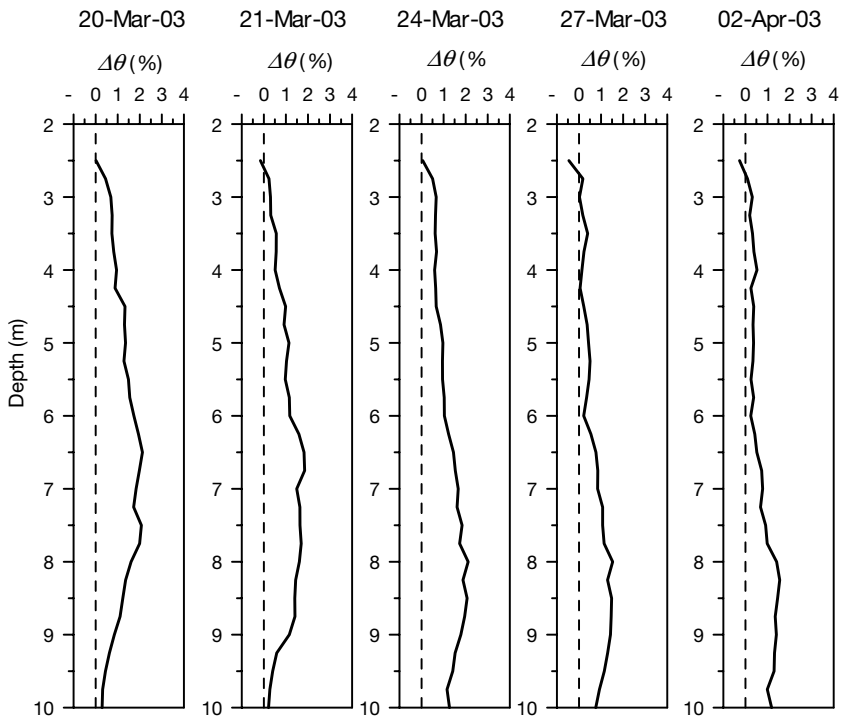
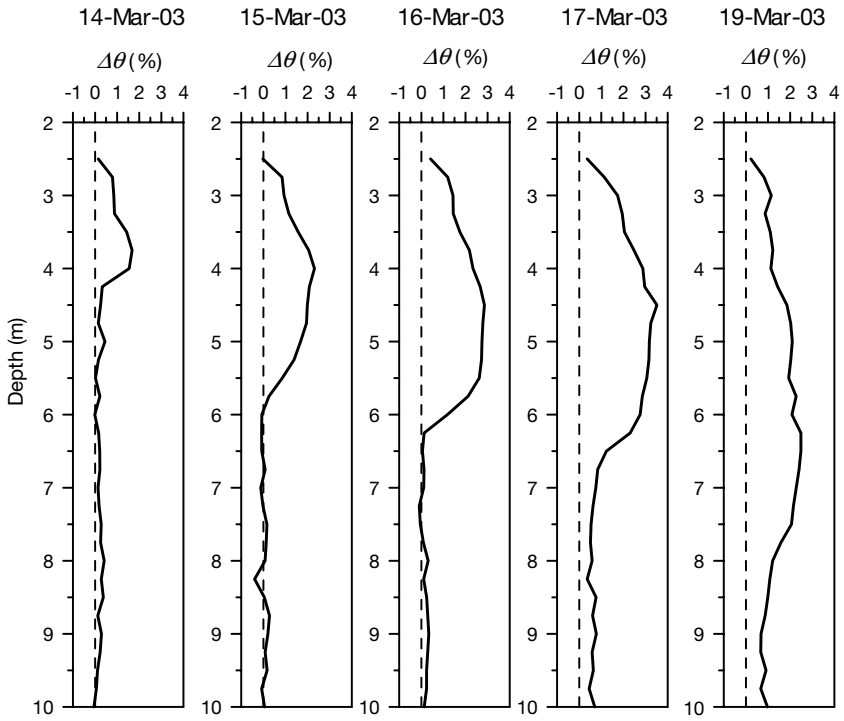


**Fig. 5.** Pre-tracer profile of dielectric constant determined from the average of ZOP surveys on 6 and 14 March 2003.



radar profile may be interpreted as follows. The high dielectric constant at 2.5 m depth is likely to be due to moisture retention at the base of the drift. At approximate depths of 4.2, 6.5 and 7.7 m increases in dielectric constant are seen, which are probably a result of further moisture retention by fine-grained units. These positions coincide with observed contrasts in the natural gamma logs shown in Figure 4 and the lithology of cores shown in Figure 3. Increases in the dielectric constant at depths greater than 9 m are also likely to be the result of increased moisture retention but also will be due to the close proximity of the water table (10 m depth). Refraction of radar waves at the water table–capillary fringe can result in apparent high radar velocities as the first arrival may be a refracted wave, rather than the assumed direct wave.

*Changes in moisture content inferred from radar measurements*

As changes in radar velocity are not dependent on lithological parameters in the petrophysical model (see equation 5), changes in moisture content may be determined more reliably. Changes in moisture content from the pre-tracer conditions, inferred from the ZOP surveys, are shown in Figure 6. The development of the tracer plume during the injection (14–17 March) is clearly seen, as is the steady vertical migration of the wetting front. As this wetting front moves, the moisture ‘bulb’ grows and thus the volumetric change in water content observed by the radar decreases over time. The volume of the subsurface that is ‘sensed’ by the radar profile is described by the Fresnel zone for the particular radar wave frequency (Cervany & Soares 1992). The Fresnel zone is assumed to be an ellipse with a minor axis length of:

$$B = \left( \frac{\lambda^2}{4} + L \times \lambda \right)^{0.5} \quad (6)$$

and a major axis length of

$$A = \left( \frac{\lambda}{4} + L \right) \quad (7)$$

where  $L$  is the borehole separation (5 m) and  $\lambda$  is the wavelength (for a 100 MHz wave, with a velocity of about 0.1 m ns<sup>-1</sup>, this is 1 m). For the

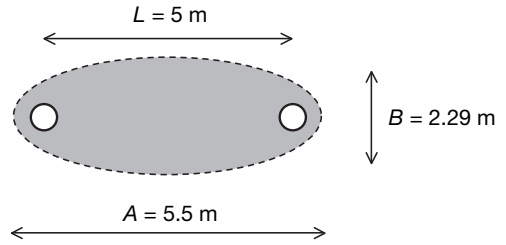


**Fig. 7.** Definition of the Fresnel zone for borehole radar measurements.

case reported here,  $B = 2.29$  m and  $A = 5.5$  m (Fig. 7).

The changes in moisture content, determined from the ZOP surveys, are shown in Figure 8 as hydrographs at particular depths. These time series reveal that approximately 230 h (about 9 days) after injection of the tracer was terminated (i.e. about 300 h after the start of tracer injection) moisture content at depths of 5 and 6 m return to near pre-tracer levels. At greater depths, however, the retention of moisture is observed for considerably longer. We infer this to be a result of fine-grained units between 8 and 9 m depth (Figs 3 and 4).

*Changes in resistivity*

The changes in moisture content determined from the radar profiles offer some insight into the mechanisms controlling unsaturated flow within the sandstone at the site. However, it is impossible to determine travel times of ‘parcels’ of water directly from these observations. Moisture already retained in the sandstone will be displaced by tracer water, but clearly ‘new’ and ‘old’ water cannot be differentiated. It is for this reason that electrical resistivity surveys were utilized. As already stated, changes in resistivity will be related to changes in moisture content and pore-water electrical conductivity (equation 3). With appropriate petrophysical relationships we may therefore use ERT and radar jointly to differentiate the ‘new’ tracer water from the existing formation water.

The changes in resistivity throughout the tracer test are shown in Figure 9. These are shown as isosurfaces of volumes with changes relative to the pre-tracer conditions above a certain threshold (in this case 7.5% for illustration of significant changes in moisture

**Fig. 6.** Changes in moisture content from pre-tracer conditions between boreholes H-R1 and H-R2 during tracer test, inferred from ZOP surveys.

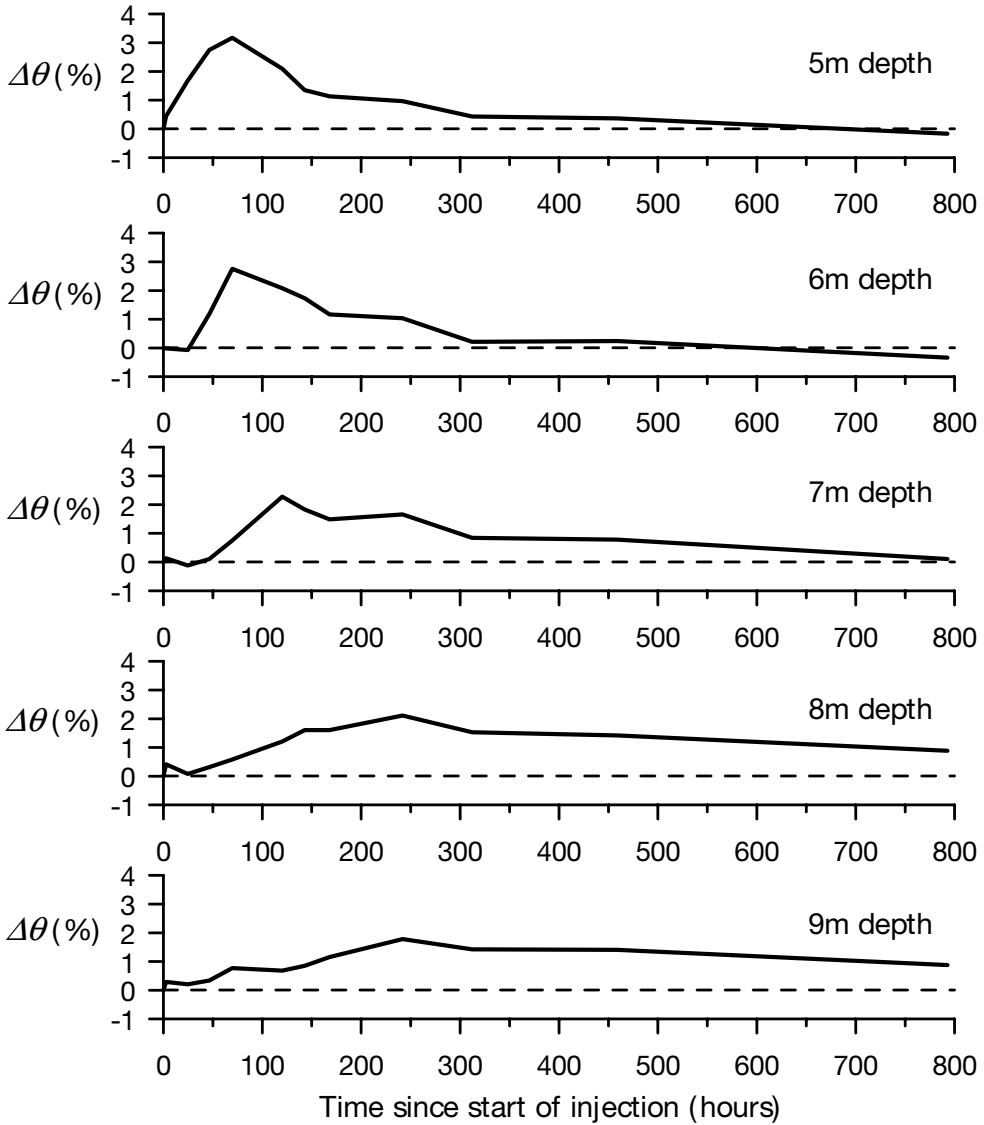


**Fig. 8.** Changes in moisture content during the tracer test at specific depths, inferred from ZOP surveys.

content). The images show clearly the development of the tracer 'bulb' during the injection and the subsequent vertical migration. Most striking is the obvious lateral spreading of the tracer between 8 and 9 m depth. These support the earlier hypothesis of a hydraulically retarding 'layer' at this depth. Note also, in Figure 9, that near the tracer-injection source (between depths of 3.5 and 6 m) the resistivity does not return to pre-tracer values even by 2 April. The volume apparently occupied by the tracer in this depth interval does shrink over the monitoring

period but is still detectable 16 days after the tracer injection was stopped. To depths of 6 m, the moisture content has returned to pre-tracer levels by 27 March (Fig. 6); the change in resistivity is thus an indication that some fraction of the pore space has been replaced by the more electrically conductive tracer fluid.

#### *Changes in pore-water solute concentration*

If we assume that the solute concentration of pore water is linearly related to the fluid

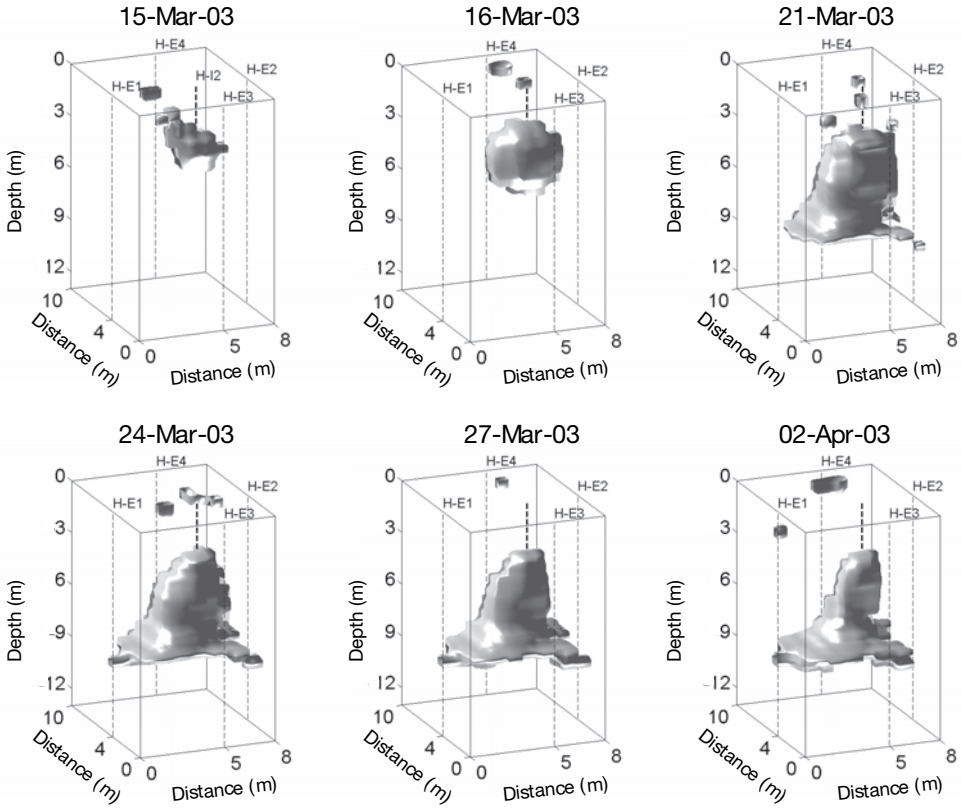


**Fig. 9.** Changes in resistivity during tracer test shown as isosurfaces of 7.5% reduction in resistivity relative to pre-tracer conditions. Shading is used to illustrate the shape of the moisture bulb that develops during the test.

electrical conductivity, i.e. inversely related to the fluid resistivity  $\rho_w$ , and given that  $\kappa_w$  will not change over time, then equations 3 and 4 can be combined to give an expression for the solute concentration relative to the background (pre-tracer) levels:

$$\frac{c_t}{c_0} = \frac{\rho_0}{\rho_t} \left( \frac{\sqrt{\kappa_0 + \phi(\sqrt{\kappa_s} - \sqrt{\kappa_a})} - \sqrt{\kappa_s}}{\sqrt{\kappa_t + \phi(\sqrt{\kappa_s} - \sqrt{\kappa_a})} - \sqrt{\kappa_s}} \right)^n \quad (8)$$

where  $C_0$  and  $C_t$  represents the solute concentration at time 0 and time  $t$ ,  $\kappa_0$  and  $\kappa_t$  are the dielectric constant values at time 0 and time  $t$ .

Assuming a value of  $n = 1.13$  (Binley *et al.* 2002b) and other values defined as before, the resistivity quotients ( $\rho_0/\rho_t$ ) were interpolated from the ERT images onto the vertical plane between radar boreholes H-R1 and H-R2. Then, using changes in dielectric constant obtained from the MOG radar inversions, the ratios of the pore water solute concentrations were

computed. The result is shown in Figure 10, from which it is apparent that the solute migrates at a much slower rate than the moisture front (as expected). Early transport is rapid to a depth of 6 m, at which point vertical transport is retarded somewhat – again supporting the hypothesis that the observed fine-grained units act as hydraulically impeding layers. We recognize that the results produced from application of equation 8 are subject to errors; increases in concentration *above* the tracer-injection zone, for example, are apparent in Figure 10. We also recognize that tomographic images are subject to inherent non-uniqueness. Nevertheless, this analysis offers some insight into unsaturated zone solute-transport processes that could not have been achieved without joint application of radar and resistivity.

### Hydrological simulations

Binley *et al.* (2002a) applied a numerical model of unsaturated flow to tracer test data at the

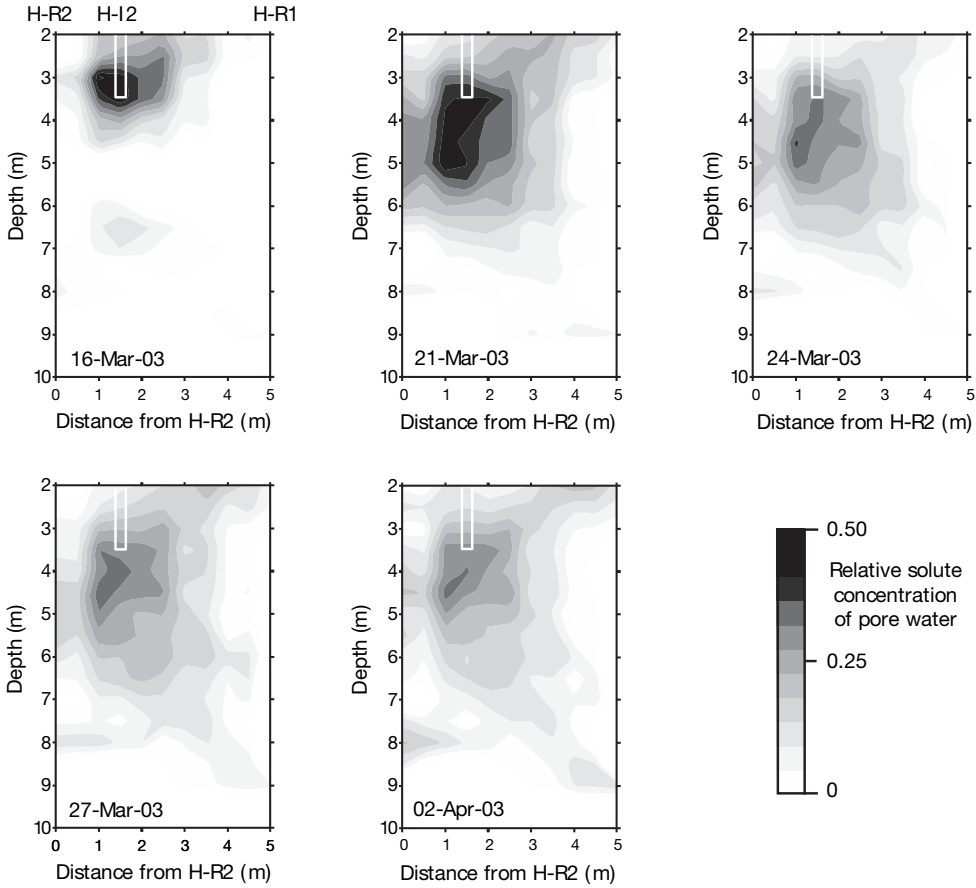


**Fig. 10.** Changes in pore-water solute concentration during the tracer test, inferred from radar and resistivity images.

Hatfield site. In their analysis the Richards equation was used, which can be written as:

$$\frac{\partial}{\partial x_i} \left( K(\psi) \frac{\partial h}{\partial x_i} \right) = \frac{\partial \theta(\psi)}{\partial t}, i = 1, 2, 3 \quad (9)$$

where  $x_i$  are the co-ordinates ( $x_3$  vertical co-ordinate),  $K(\psi)$  is the hydraulic conductivity,  $\psi$  is the pressure head,  $h$  is the hydraulic head =  $\psi + x_3$ ,  $\theta(\psi)$  is volumetric moisture content and  $t$  is time.

In the analysis of Binley *et al.* (2002a) it was assumed that the unsaturated sandstone could be represented by a single effective hydrogeological unit and attempts were made to determine appropriate hydraulic parameters for the Hatfield site. The tracer test used was restricted in duration to approximately 200 h, i.e. 25% of that presented here. In an attempt to extend the

findings of this earlier study we apply here the same numerical parameterization as Binley *et al.* (2002a) and compare the simulated response with observations.

Modelling of the unsaturated zone was carried out using the three-dimensional (3D) finite-element model FEMWATER (Lin *et al.* 1997), which is based on a pressure head formulation. In FEMWATER, the widely used van Genuchten model (van Genuchten 1980) describing the unsaturated hydraulic relationships is adopted. With such an approach the unsaturated characteristics are described by:

$$\theta(\psi) = \theta_r + \frac{\theta_s - \theta_r}{[1 + |\alpha\psi|^\beta]^\beta} \quad (10)$$

and

$$K(\psi) = K_s S_e^{0.5} \left[ 1 - (1 - S_e^{\beta/(\beta-1)})^{\frac{\beta-1}{\beta}} \right]^2 \quad (11)$$

where  $K_s$  is the saturated hydraulic conductivity,  $\theta_r$  is the residual moisture content,  $\theta_s$  is the saturated moisture content,  $S_e$  is effective saturation ( $= (\theta - \theta_r)/(\theta_s - \theta_r)$ ), and  $\alpha$  and  $\beta$  are parameters.

As in Binley *et al.* (2002a), a model was set up to represent a parallelepiped of 11 × 11 m in plan (to allow specification of zero horizontal flow-boundary conditions) and 10 m in depth. The system was composed of three layers (Table 1): upper soil (Layer 1), sandy soil (drift) (Layer 2) and sandstone (Layer 3). The injection took place in Layer 3. The mesh model was composed of about 125 000 six-node prism elements and 65 000 nodes. The solution to the system of non-linear equations was achieved with a convergence threshold for hydraulic head equal to 0.001 m. The total simulation time was 500 h.

Figure 11 shows the observed and simulated change in volume of water in the system. In this figure the observed changes are inferred from the ZOP radar profiles. The total injected volume is 1.2 m<sup>3</sup>, but because radar transmission paths do not cover the entire volume invaded by the tracer a mass balance error results. This ‘error’ increases with time as the moisture bulb spreads laterally orthogonal to the radar transmission plane. The observed response shows a sharp increase in water volume (as the tracer is injected), followed by a slower decrease as the sampled volume drains. Note that some scatter is seen in the recession limb of the hydrograph, which is inevitable given that the observed changes in moisture content are very low (Fig. 6).

Equations 6 and 7 were used to define the appropriate sampling volume for the numerical simulations. From Figure 11 it is apparent that the model and observed responses match very well until approximately 200 h into the tracer test. After this point the model underpredicts the water volume within the Fresnel zone,

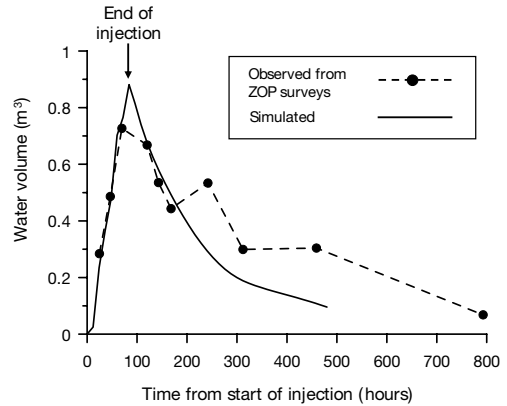


**Fig. 11.** A comparison of measured and modelled pore-water volumes between H-R1 and H-R2 during the tracer test.

implying that in the model drainage to the water table is too rapid. Interestingly, the optimization of effective hydraulic parameters by Binley *et al.* (2002a) was constrained to 250 h; it appears that, given extended data for the 2003 tracer test, parameterization of the deeper sandstone is inappropriate. This again supports the hypothesis that a low hydraulic conductivity unit exists deeper in the profile, for example at 8–9 m. It appears, therefore, that a single effective hydraulic conductivity value is not appropriate for the sandstone.

**Conclusions**

Cross-borehole radar and resistivity measurements have been used to characterize changes in moisture content and solute concentration due to controlled injection of a saline tracer in the unsaturated zone of the Sherwood Sandstone. Borehole radar transmission profiles show the vertical migration of the wetting front during the tracer test. Changes down to 1% volumetric moisture content appear detectable by the technique used, although we recognize

**Table 1.** Hydraulic parameters for unsaturated flow modelling at the Hatfield site (after Binley *et al.* 2002a)

	$\theta_r$	$\theta_s$	$\beta$	$\alpha$ (m <sup>-1</sup> )	$K_s$ (m day <sup>-1</sup> )
Layer 1 (0–0.5 m bgl)*	0.05	0.30	1.9	2	0.01
Layer 2 (0.5–3 m bgl)	0.04	0.32	2.2	2	0.048
Layer 3 (3–12 m bgl)	0.04	0.32	2.5	10	0.4 <sup>†</sup>

\* m bgl, metres below ground level.

<sup>†</sup> The  $K_s$  in this layer is based on the optimum value determined by Binley *et al.* (2002a).

that such signal sensitivity will not be achievable at all field sites. Three-dimensional cross-borehole electrical resistivity tomography was deployed to monitor changes in resistivity over time. The results show clearly the plume development and have revealed the impact of a hydraulically impeding layer above the water table. Geophysical and geological logs acquired at the site support this conceptualization. By combining the resistivity tomograms with cross-borehole radar tomograms we have estimated changes in pore-water concentration over time, albeit in a 2D vertical plane. Such information would not be obtainable without the joint application of radar and resistivity methods. By utilizing these in cross-borehole mode high-resolution imaging has been achievable.

In many previous hydrogeological studies geophysical techniques have been adopted in a purely qualitative manner. There is, however, hydraulic information that can be extracted from these techniques through appropriate integration with a hydrological modelling program. We have demonstrated how numerical models may be used jointly with geophysics and believe that further hydrogeophysical studies will show the immense value of geophysical data in constraining subsurface hydrological models. Our conceptual and numerical models of unsaturated flow and transport processes in the Sherwood Sandstone will continue to be refined and, we believe, ultimately help constrain predictive models used by water-resource managers and environment regulators.

We are grateful to the Environment Agency, UK, for continued support for our work. E. Mould and A. Walmsley (Environment Agency, UK) brought drilling expertise early on in the project. The work would not have been possible without agreement of site access by J. Cunliffe of Lings Farm, Hatfield. J. West supplied core logs and saturation–Dc resistivity data. This work was funded by the Natural Environment Research Council, UK, under NERC studentship grant NER/S/A/2001/06246.

## References

ALUMBAUGH, D., CHANG, P.Y., PAPROCKI, L., BRAINARD, J.R., GLASS, R.J. & RAUTMAN, C.A. 2002. Estimating moisture contents in the vadose zone using cross-borehole ground penetrating radar: A study of accuracy and repeatability. *Water Resources Research*, **38**, 1309, doi:10.1029/2001WR000754.

ARCHIE, G.E. 1942. The electrical resistivity log as an aid to determining some reservoir characteristics. *Transactions of the American Institute of Mining Engineers*, **146**, 389–409.

BINLEY, A. & BEVEN, K. 2003. Vadose zone flow model

uncertainty as conditioned on geophysical data. *Ground Water*, **41**, 119–127.

BINLEY, A., CASSIANI, G., MIDDLETON, R. & WINSHIP, P. 2002a. Vadose zone model parameterisation using cross-borehole radar and resistivity imaging. *Journal of Hydrology*, **267**, 147–159.

BINLEY, A., CASSIANI, G. & WINSHIP, P. 2004. Characterization of heterogeneity in unsaturated sandstone using borehole logs and cross-borehole tomography. In: BRIDGE, J.S. & HYNDMAN, D.W. (eds) *Aquifer Characterization by SEPM*. Society for Sedimentary Geology, Tulsa, OK, 129–138.

BINLEY, A., WINSHIP, P., MIDDLETON, R., POKAR, M. & WEST, J. 2001. High resolution characterization of vadose zone dynamics using cross-borehole radar. *Water Resources Research*, **37**, 2639–2652.

BINLEY, A., WINSHIP, P., WEST, L.J., POKAR, M. & MIDDLETON, R. 2002b. Seasonal variation of moisture content in unsaturated sandstone inferred from borehole radar and resistivity profiles. *Journal of Hydrology*, **267**, 160–172.

CERVANY, V. & SOARES, J.E.P. 1992. Fresnel volume ray tracing. *Geophysics*, **57**, 902–915.

DAILY, W., RAMIREZ, A., BINLEY, A. & LABRECQUE, D. 2004. Electrical resistance tomography. *The Leading Edge*, **23**, 438–442.

DAILY, W.D., RAMIREZ, A.L., LABRECQUE, D.J. & NITAO, J. 1992. Electrical resistivity tomography of vadose water movement. *Water Resources Research*, **28**, 1429–1442.

FRENCH, H.K., HARDBATTLE, C., BINLEY, A., WINSHIP, P. & JAKOBSEN, L. 2002. Monitoring snowmelt induced unsaturated flow and transport using electrical resistivity tomography. *Journal of Hydrology*, **267**, 273–284.

GALAGEDARA, L.W., PARKIN, G.W., REDMAN, J.D. & ENDRES, A.L. 2003. Assessment of soil moisture content measured by borehole GPR and TDR under transient irrigation and drainage. *Journal of Environmental Engineering and Geophysics*, **8**, 77–86.

HUBBARD, S.S., PETERSON, J.E., MAJER, E.L., ZAWISLANSKI, P.T., WILLIAMS, K.H., ROBERTS, J. & WOBBER, F. 1997. Estimation of permeable pathways and water content using tomographic radar data. *Leading Edge*, **16**, 1623–1628.

JACKSON, M.J. & TWEETON, D.R. 1994. *MIGRATOM – Geophysical Tomography Using Wavefront Migration and Fuzzy Constraints*. Bureau of Mines Report, **R19497**.

LABRECQUE, D.J., MILLETO, M., DAILY, W., RAMIREZ, A. & OWEN, E. 1996. The effects of noise on Occam's inversion of resistivity tomography data. *Geophysics*, **61**, 538–548.

LIN, H.J., RICHARDS, D.R., TALBOT, C.A., YEH, G.T., CHENG, J. & CHENG, H. 1997. *FEMWATER: A Three-dimensional Finite Element Computer Model for Simulating Density-dependent Flow and Transport in Variably Saturated Media*. US Army Corps of Engineers and Pennsylvania State University Technical Report, **CHL-97-12**.

MORELLI, G. & LABRECQUE, D.J. 1996. Advances in ERT modelling. *European Journal of Environmental and Engineering Geophysics*, **1**, 171–186.

- PETERSON, J. 2001. Pre-inversion corrections and analysis of radar tomographic data. *Journal of Environmental and Engineering Geophysics*, **6**, 1–18.
- POKAR, M., WEST, L.J., WINSHIP, P. & BINLEY, A.M. 2001. *Proceedings of the Symposium on Applications of Geophysics to Engineering and Environmental Problems (SAGEEP2001)*. Environmental and Engineering Geophysical Society, Denver, CO.
- RAMIREZ, A. & DAILY, W. 2001. Electrical imaging at the large block test – Yucca Mountain, Nevada. *Journal of Applied Geophysics*, **46**, 85–100.
- RUBIN, Y. & HUBBARD, S.S. 2005. *Hydrogeophysics*. Springer, New York.
- SLATER, L., ZAIDMAN, M.D., BINLEY, A.M. & WEST, L.J. 1997. Electrical imaging of saline tracer migration for the investigation of unsaturated zone transport mechanisms. *Hydrology and Earth System Science*, **1**, 291–302.
- VAN GENUCHTEN, M.T. 1980. A closed-form equation for predicting the hydraulic conductivity of unsaturated soils. *Soil Science Society of America Journal*, **44**, 892–898.
- WEST, L.J., HANDLEY, K., HUANG, Y. & POKAR, M. 2003. Radar frequency dielectric dispersion in sand and sandstone: Implications for determination of moisture content and clay content. *Water Resources Research*, **39**, 1026, doi:10.1029/2001WR000923.
- WORTHINGTON, P.F. 1977. Influence of matrix conduction upon hydrogeophysical relationships in arenaceous aquifers. *Water Resources Research*, **13**, 87–92.